

E1-E2 interference in the vuv photoionization of HeE. P. Kanter, B. Krässig, and S. H. Southworth
*Argonne National Laboratory, Argonne, Illinois 60439, USA*R. Guillemin, O. Hemmers, and D. W. Lindle
*Department of Chemistry, University of Nevada, Las Vegas, Nevada 89154, USA*R. Wehlitz
*Synchrotron Radiation Center, University of Wisconsin, Stoughton, Wisconsin 53589, USA*M. Ya. Amusia
*Racah Institute of Physics, The Hebrew University, Jerusalem 91904, Israel
and Ioffe Physical-Technical Institute, St. Petersburg 194021, Russia*L. V. Chernysheva
*Ioffe Physical-Technical Institute, St. Petersburg 194021, Russia*N. L. S. Martin
Department of Physics and Astronomy, University of Kentucky, Lexington, Kentucky 40506, USA
(Received 18 February 2003; published 22 July 2003)

We have measured the forward-backward asymmetry of photoelectron angular distributions produced in the vacuum ultraviolet photoionization of helium. This asymmetry, a consequence of the breakdown of the dipole approximation, measures the real part of the ratio of the quadrupole and dipole matrix elements. In the autoionization region, the strong energy dependence of the asymmetry permits an experimental separation of the ratio of those magnitudes from their phase difference. We experimentally determined the Fano parameters of the $2p^2\ ^1D_2$ quadrupole resonance, and report improved values of the width Γ and line profile parameter q from those previously available from electron scattering. Off resonance, the smooth energy dependence of the asymmetry is found to agree well with the theoretical treatment presented here which incorporates higher-multipole effects.

DOI: 10.1103/PhysRevA.68.012714

PACS number(s): 32.80.Dz, 32.30.Jc

I. INTRODUCTION

At low photon energies, atomic photoabsorption is usually well described by the dipole approximation in which the photon field

$$\exp(i\mathbf{k}\cdot\mathbf{r}) \approx 1 + i\mathbf{k}\cdot\mathbf{r} + \dots \quad (1)$$

is approximated by unity (\mathbf{k} is the photon propagation vector and \mathbf{r} is the electron position vector). For photon energies in the vacuum ultraviolet, this is an excellent approximation in calculating total cross sections [1]. Breakdown of this approximation, however, can be observed by investigating photoelectron angular distributions [2,3]. This is because the higher-order terms of this expansion are analogous to the higher multipoles of the classical radiation theory [4] and thus contribute additional terms to the differential cross section which vanish (or become negligible) when integrated over all angles but can be enhanced by specific geometries [5]. Measurements of the fore-aft asymmetry of photoelectrons emitted in the forward and backward hemispheres (with respect to \mathbf{k}) have demonstrated a particularly sensitive probe of the contribution of higher-order terms [6,7] because in the dipole approximation all dependence on the photon propagation direction vanishes. This dependence on the

beam direction has long been known at high energies where the dipole approximation is expected to fail [8]. Later, it was suggested that, in some cases, those effects could become significant even close to an outer subshell ionization threshold [9]. Recently, such nondipole effects have been observed at a very low photon energy (150 eV) in neon valence photoelectron angular distributions [10], and theoretical predictions have now been made for the size of such effects in rare gas atoms down to threshold [11–16].

Ever since Heisenberg's 1926 attempt to apply the "new quantum theory" to it [17], the helium atom has served as a prototypical test bench of the atomic theory. Experimentally, as the lightest rare gas, it is relatively easy to handle as a target atom for photon or particle interaction studies. Theoretically, it is the simplest two-electron system and has thus played a pivotal role in our understanding of correlated electron dynamics [18]. Furthermore, for helium, the energy of any state in which both electrons are excited is higher than the ionization threshold and thus such states appear as autoionizing continuum resonances. The autoionization continuum of He has been studied in great detail for nearly 40 years, beginning with the pioneering work of Madden and Codling [19]. More recently, there have been several extensive high-resolution photoionization studies of many of these resonances [20–25]. All of that work, however, has been limited to $J=1$ dipole-excited resonances.

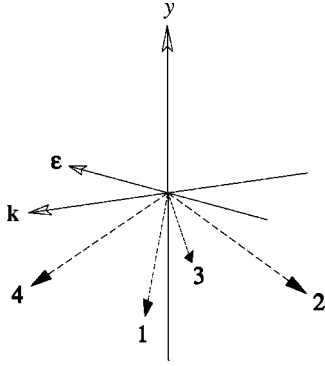


FIG. 1. (Color online) Schematic arrangement of the experimental apparatus. The photon propagation vector \mathbf{k} (or \hat{x} direction), polarization vector $\boldsymbol{\epsilon}$ (or \hat{z} direction), and gas jet axis \hat{y} were mutually orthogonal. The four electron spectrometers (1–4) were positioned at polar angles of θ_m and $180^\circ - \theta_m$ and azimuthal angles of 225° and 315° , respectively. For the permutation shown here the (θ, ϕ) coordinates of each detector are 1: $(180 - \theta_m, 315)$, 2: $(180 - \theta_m, 225)$, 3: $(\theta_m, 225)$, and 4: $(\theta_m, 315)$.

Recently, it was shown that the $2p^2\ ^1D_2$ quadrupole resonance in He could be observed in photoionization by measuring the nondipole photoelectron asymmetry [26]. Here we present a more extensive report on the nondipole asymmetries of He photoelectrons encompassing the $2s2p\ ^1P_1$ and $2p^2\ ^1D_2$ autoionizing resonances (~ 60 eV) as well as the nonresonant photoionization regions at lower and higher energies. Specifically, we report here our measurements of the photoelectron angular asymmetry over the photon energy range from 10 eV above threshold (24.587 eV) to 160 eV. Comparisons are made with both of the recent theoretical calculations [11,12]. Some of the numerical computations of Ref. [12] were repeated with improved accuracy and those results are presented here.

II. THEORY

Keeping the second term in the exponential expansion [Eq. (1)] and neglecting terms of $O(\alpha^2)$, where α is the fine structure constant, several authors [12–16] have shown that the resulting interference between the electric dipole $E1$ and the electric quadrupole $E2$ photoionization amplitudes contributes a term to the differential cross section of the form $\langle xz \rangle \langle z \rangle^* + \langle z \rangle \langle xz \rangle^*$, where $\langle z \rangle$ and $\langle xz \rangle$ correspond to the $E1$ and $E2$ matrix elements, respectively, for a set of coordinate axes such that the photon beam is incident in the positive x direction with the linear polarization along the z axis (see Fig. 1). Magnetic dipole ($M1$) terms could also contribute in first order in α through $E1$ - $M1$ interference, but in a nonrelativistic independent particle model, $M1$ amplitudes vanish [16] and furthermore have been shown to be negligible below 5 keV even in relativistic treatments with an initial s subshell [11].

Whereas the dipole approximation (with cross section $\sigma_1 \propto \langle z \rangle \langle z \rangle^*$) contributes terms to the differential cross section which are only even in $\cos(\theta)$, the $E1$ - $E2$ interference contributes a term proportional to $\sin(\theta)\cos(\phi)$ and hence is

asymmetric with respect to the beam propagation vector \mathbf{k} . Here, θ is the polar angle of the photoelectron momentum vector \mathbf{p} with respect to the photon polarization axis $\boldsymbol{\epsilon}$ and ϕ is the azimuthal angle between \mathbf{k} and the projection of \mathbf{p} in the plane perpendicular to $\boldsymbol{\epsilon}$. Factoring out the usual dipole cross section from the interference term yields the following expression:

$$\frac{\langle xz \rangle \langle z \rangle^* + \langle z \rangle \langle xz \rangle^*}{\langle z \rangle \langle z \rangle^*} = 2\text{Re} \left\{ \frac{\langle xz \rangle}{\langle z \rangle} \right\}. \quad (2)$$

Using this, the general form of the photoelectron angular distribution has been given by Cooper [16] for s electrons and 100% linear polarization in the form

$$\frac{d\sigma(\theta, \phi)}{d\Omega} = \frac{\sigma_1}{4\pi} [1 + \beta P_2(\cos \theta) + \gamma \cos^2 \theta \sin \theta \cos \phi]. \quad (3)$$

The first two terms represent the dipole contribution characterized by the dipole anisotropy parameter β and the last term [of $O(\alpha\omega)$ relative to the dipole terms], resulting from Eq. (2), is the result of $E1$ - $E2$ interference and is quantified in terms of the parameter γ which is then simply

$$\gamma = 3\alpha\omega \frac{Q}{D} \cos(\delta_2 - \delta_1), \quad (4)$$

where ω is the photon energy, D, Q are the magnitudes of the dipole and quadrupole matrix elements, and $\delta_{1,2}$ are the phase shifts of the E_p, E_d continuum states of photoelectron energy E [14–16]. Note that all quantities are expressed in atomic units.

At the “magic angles” $\theta = \theta_m \approx 54.74^\circ$ and $180^\circ - \theta_m$ [where $P_2(\cos \theta_m) = 0$], the contribution of the β term vanishes and the expression further simplifies to

$$\frac{d\sigma(\theta_m, \phi)}{d\Omega} = \frac{\sigma_1}{4\pi} \left(1 + \gamma \sqrt{\frac{2}{27}} \cos \phi \right). \quad (5)$$

For electron spectra measured at the same polar angle but in opposite directions with respect to the beam direction (see Fig. 1), $\cos \phi$ changes sign. Thus, the *difference* between such pairs of spectra isolates the interference term and γ . By contrast, the nondipole term vanishes in the *sum* of such spectra yielding only the pure dipole cross section [27,28].

A. Global behavior

It has been shown that for He, near threshold, $\gamma \sim \alpha$ [29] and is thus very small. For photon energies large in comparison with the electron binding energy of He (24.587 eV), further simplification is possible by employing the Born approximation for the outgoing electron. This avoids the multipole expansion and treats retardation effects [4] to all orders. In the plane-wave Born approximation, the absorbed photon transfers all of its momentum to the ejected photoelectron skewing the angular distribution forward in the direction of the beam [4]. This results in the high-energy limit of γ tending toward $12v/c \sim \alpha\sqrt{\omega}$, where v is the photoelec-

tron velocity and c is the speed of light. Thus, at low energies, the parameter γ is small and varies smoothly with ω . It can, however, be enhanced when \mathcal{D} becomes vanishingly small or \mathcal{Q} becomes large—conditions that can be met near dipole and quadrupole autoionizing resonances.

B. Effect of autoionization

We have previously reported on autoionization effects observed in the nondipole asymmetry parameter γ in He [26]. Here we present additional details of the derivation of the expression for γ in the region of an autoionization resonance. This requires the application of Fano's formulation [30–32] of the resonance profile in total cross sections. Similar extensions of the Fano formula have previously been given for partial cross sections and branching ratios [33] and for the β parameter and photoelectron spin polarization [34].

As discussed above, in regions of the photoionization spectrum where no autoionizing levels are present, the quantities \mathcal{D} , \mathcal{Q} , and $\delta_{1,2}$ are all slowly varying functions of energy. When autoionization is present, the general form of Eq. (4) remains the same but these parameters are now strong functions of energy in the neighborhood of the autoionizing resonances [30]. Here we restrict the discussion to the simple case of a single resonance interacting with a single continuum channel which is sufficient to describe our measurements of γ through the He $2s2p\ ^1P_1$ and $2p^2\ ^1D_2$ autoionizing levels near 60 eV.

Fano showed that for a single autoionizing resonance at ω_0 coupled to a single continuum, the transition amplitude should be multiplied by the factor

$$\frac{q+\varepsilon}{i+\varepsilon} = \frac{(q+\varepsilon)}{(1+\varepsilon^2)^{1/2}} \exp(i\Delta), \quad (6)$$

where

$$\cot \Delta = -\varepsilon, \quad (7a)$$

$$\varepsilon = \frac{\omega - \omega_0}{\Gamma/2}. \quad (7b)$$

Writing $\mathcal{D} = \mathcal{R}_1$, $\mathcal{Q} = \mathcal{R}_2$ and labeling resonant quantities with the superscript R and the channel ℓ ($= 1$ or 2), multiplication of this resonant factor with the nonresonant amplitude gives

$$\mathcal{R}_\ell^R = \mathcal{R}_\ell \frac{(q_\ell + \varepsilon_\ell)}{(1 + \varepsilon_\ell^2)^{1/2}}, \quad (8)$$

$$\delta_\ell^R = \delta_\ell + \Delta_\ell. \quad (9)$$

Here, q_ℓ is the Fano q parameter of the resonance, ε_ℓ is the energy away from the resonance position ω_ℓ measured in units of the halfwidth $\Gamma_\ell/2$ of the resonance, and Δ_ℓ is the extra phase shift due to autoionization. In Eq. (3), the dipole cross section is replaced by the resonant form

$$\sigma_1^R = \sigma_1 \frac{(q_1 + \varepsilon_1)^2}{(1 + \varepsilon_1^2)}, \quad (10)$$

and, for the ionization of s electrons, a resonant value of γ^R may be written in terms of the γ_0 that would exist at ω if autoionization was not present as

$$\gamma^R = \gamma_0 \left\{ \frac{\cos(\delta_2 - \delta_1 + \Delta_2 - \Delta_1)}{\cos(\delta_2 - \delta_1)} \right\} \times \left\{ \frac{(q_2 + \varepsilon_2)}{(1 + \varepsilon_2^2)^{1/2}} \right\} / \left\{ \frac{(q_1 + \varepsilon_1)}{(1 + \varepsilon_1^2)^{1/2}} \right\}. \quad (11)$$

For the general case of arbitrary angular momenta, a similar expression has been given by Amusia *et al.* [35].

In helium, the autoionizing levels $2s2p\ ^1P_1$ and $2p^2\ ^1D_2$ lie close together at about 60 eV above the $1s^2\ ^1S_0$ ground state. They are accessible by an electric dipole and electric quadrupole transition, and autoionize into the $1sE_p\ ^1P_1$ and $1sEd\ ^1D_2$ continua, respectively. In our experiment, we have measured the energy dependence of both the cross section and the nondipole asymmetry parameter γ in the vicinity of these resonances. Though relatively close, these resonances are sufficiently well separated (~ 250 meV which is more than four times the level width) that the resonant effects on \mathcal{Q} and \mathcal{D} can be observed individually and used to isolate the nonresonant \mathcal{Q}/\mathcal{D} ratio from the cosine factor in Eq. (4).

III. EXPERIMENT

The experiment was carried out at the University of Wisconsin's Synchrotron Radiation Center (SRC) on the PGM Undulator 071 beam line. The first-order linearly polarized radiation from the undulator was monochromatized with a plane grating monochromator using 50- μ m slits giving a bandpass of ≈ 20 meV. The beam flux was monitored by measuring the current produced by the passage through a nickel mesh. The beam (focused to 0.7×0.075 mm²) then entered a doubly μ -metal-shielded vacuum chamber housing four parallel plate electron analyzers (PPAs). The PPAs were mounted on a rotation stage with rotation axis (the \hat{y} -axis) perpendicular to the photon beam (see Fig. 1). The spectrometers were at fixed polar angles corresponding to the "magic angles" described above and 90° apart in azimuthal angles corresponding to 225° and 315° . By rotation of the mounting stage, the spectrometers could be permuted and thus each PPA was situated at all four of those observation angles. Thus, with four rotations at each energy, we carried out redundant measurements of the forward-backward asymmetry, which were then averaged. This averaging procedure served to eliminate the dependence of the measured asymmetries on the polarization properties of the photon beam [36]. On the rotation axis of the stage, an effusive gas jet, positioned at ≈ 1 mm below the photon beam, intersected the photons at the common source point of the four PPAs. In this geometry, the 1-cm-long analyzing slits of each spectrometer had the same projection on the interaction region defined by that intersection. Also on the rotation axis, in the opposing direc-

tion, an ion detector viewed the interaction region from above and, with a weak electric field ($\ll 1$ V/cm), extracted photoions produced by the beam. This detector was a channel electron multiplier operated in current mode.

The PPA spectrometers were operated in a constant pass-energy mode in which electrons from the interaction region, which entered the spectrometer nozzles, were either accelerated or decelerated to a predetermined energy of 100 eV and then analyzed at this fixed energy while the acceleration potential was varied to sweep out an energy spectrum. In this way, the kinetic energy resolution of the PPAs was fixed at ~ 2 eV and broad enough to efficiently collect the photopeak electrons.

Both cross sections and nondipole asymmetries were measured by carrying out constant ionic state (CIS) scans of the resonance region in the following manner. First, the undulator and monochromator were adjusted at the starting energy for the scan and the PPA analyzing voltages adjusted to the maximum of the photopeak. Then, under computer control, the undulator, monochromator, and PPAs were adjusted in equal energy steps across the photon energy range of interest. The spectrometers were then rotated by 90° and the CIS scan repeated, four times, so that each spectrometer measured the yield at each of the four PPA positions. For each of the PPAs, the experimental γ parameters were determined from the forward-backward asymmetries measured at the four angular positions. Defining the yield measured in spectrometer position n (denoted in Fig. 1) as \mathcal{Y}_n , then from Eq. (5) these can be combined to produce a measured value of γ_m by

$$\gamma_m = \sqrt{27} \left(\frac{\mathcal{Y}_1 - \mathcal{Y}_2 - \mathcal{Y}_3 + \mathcal{Y}_4}{\mathcal{Y}_1 + \mathcal{Y}_2 + \mathcal{Y}_3 + \mathcal{Y}_4} \right). \quad (12)$$

This represents an individual measurement of the forward-backward asymmetry. These were computed for each of the four PPAs and then averaged to minimize systematic effects such as stray fields, small angular misalignments, detection efficiencies, etc. The angle-integrated cross sections were determined from the ion yield detector, which had superior statistics to the photoelectron yields from the PPAs. Further details of this apparatus and measurement procedures have been published elsewhere [36].

When, as is usually the case, the dipole cross section dominates the total cross section, the experimental γ_m can be compared directly to calculations of the quantity γ as defined in Eqs. (3) and (4). However, as higher-order multipoles become significant at high energies [36], or when the dipole amplitude vanishes (as in the case of the He dipole resonance considered here), this comparison is inappropriate since, experimentally, the total cross section includes all multipoles. When the dipole amplitude vanishes, the observed γ actually scales as \mathcal{D}/Q and remains finite as discussed in Appendix A. As a practical matter, however, our experimental energy resolution is comparable to the dipole resonance width and obscures this effect (see Appendix B), so Eq. (4) remains a good representation of the data.

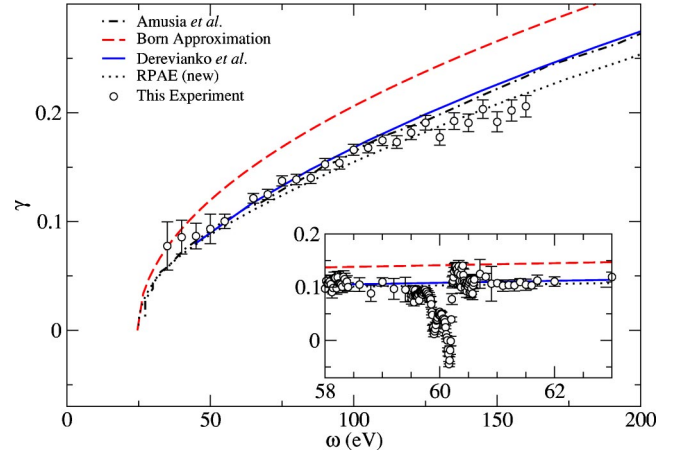


FIG. 2. (Color online) Energy dependence of asymmetry parameter γ from threshold to 160 eV. The data have been averaged over 5-eV-wide bins. The open points are the results of this experiment with statistical errors noted. The errors at the lowest energies include a systematic contribution (added linearly) describing the variation between the different measurements as described in text. The solid line is an interpolation of the calculation by Derevianko, Johnson, and Cheng [11]. The dot-dashed line is similarly interpolated to show the calculation of Amusia *et al.* [12], and the dashed curve shows the high-energy Born-approximation result. The dotted line shows the revised RPAE calculation. The inset shows the data (complete unaveraged data and calculations) with an expanded energy scale in the region of the 1P_1 and 1D_2 autoionization resonances.

IV. RESULTS AND DISCUSSION

A. Nonresonant photoionization

Figure 2 shows the measured γ values as a function of photon energy including all of the data from 35 to 160 eV. The data, mostly measured in 1 eV steps, have been averaged over bins of 5 eV width to improve statistics and reduce scatter. As seen in the inset, there is a pronounced dip in the vicinity of the $(2s2p) ^1P_1$ and $2p^2 ^1D_2$ autoionization resonances (~ 60 eV) and consequently, this region was measured with much finer steps (~ 0.01 eV). There are, of course, many other autoionization resonances [22] between this region and the double ionization limit (~ 79 eV), but these are not observed with the coarse steps used in the measurements above 62 eV. Above and below the resonance region, the data generally show a smooth monotonic rise with increasing photon energy. The experimental errors of the lowest energies (below 10 eV in photoelectron energy) grow larger because of increased scatter between measurements with the individual spectrometers. This systematic error, which grows with decreasing energy, results from weak-field inhomogeneities within the electron spectrometers and is estimated from the dispersion between the individual measurements. At higher energies (above 20 eV in photoelectron energy), this dispersion is negligible in comparison to statistical errors. At the highest energies measured, the errors are dominated by statistics and grow with increasing energy as the photoionization cross section declines.

In addition to our experimental data, Fig. 2 also shows the theoretical predictions of Derevianko *et al.* [11], Amusia *et al.* [12], and the Born approximation, along with the calculations from the present work. Derevianko *et al.* used the relativistic independent particle approximation (IPA) with a modified Hartree potential. They report a close agreement with the nonrelativistic IPA calculations of Cooper [16] who employed a Herman-Skillman potential. Amusia *et al.* [12] used both the Hartree-Fock approximation and the random phase approximation with exchange (RPAE). The new RPAE results differ slightly from those published previously [12] due to the improved accuracy of the calculations, specifically in the solution of the RPAE equations. Previous comparisons of IPA and random-phase approximation calculations of the nondipole parameters in neon have found a close agreement [11]. For photon energies ≥ 45 eV (photoelectron energies above ≥ 20 eV), we find generally a good agreement between those calculations and our experiment. For the lower-energy region, our data hint at an increase in γ , which is inconsistent with the theories. However, because of the limitations of the present apparatus at low energies as described earlier, systematic errors near threshold make it difficult to provide a test of current theories in this region. An improved apparatus is necessary to investigate the threshold region in detail. At higher energies, the new RPAE results are systematically lower than either the published RPAE [12] or the relativistic IPA results [11], and are in better agreement with the experimental data.

B. Resonance region

The resonance region was investigated with finer energy steps to elucidate the rapid energy dependence of γ and the total cross section (see Fig. 3). These data represent all of the CIS scans which were carried out in the resonance region. In addition to the CIS scans, at a few energies, γ was determined from complete photoelectron spectra measured at each orientation of the PPAs to check for consistency. These data, of somewhat lower statistical quality, are also incorporated into the data set shown in the figure. The well-known $(2s2p)^1P_1$ dipole resonance is observed at 60.15 eV with its characteristic Fano profile [30] and was used as our energy calibration standard (see Table I). The nearby quadrupole resonance, weaker by $O(\alpha^2\omega^2) \sim 3 \times 10^{-4}$, cannot be discerned in the total cross section. These data were fitted with a profile determined by the dipole cross section [Eq. (10)] convoluted with the ≈ 20 meV beam line bandpass. The line shape of the bandpass was determined in a separate measurement (see Fig. 4) of the nearby xenon $4d^95s^25p^66p^1P_1^o$ resonance at 65.11 eV [37]. This resonance has a very large q (~ 200) and hence a symmetric Lorentzian line shape [37,38]. Given the well-established resonance width [39], we have used these data to determine the spectral shape of the beam line bandpass. The resonance cross section, convoluted with that bandpass, is plotted as the solid line in Fig. 4. Using the same bandpass function, we then fitted the He cross section data as shown in the lower panel of Fig. 3. Allowing the He dipole resonance width and q_1 to vary as free parameters, we obtain an excellent agree-

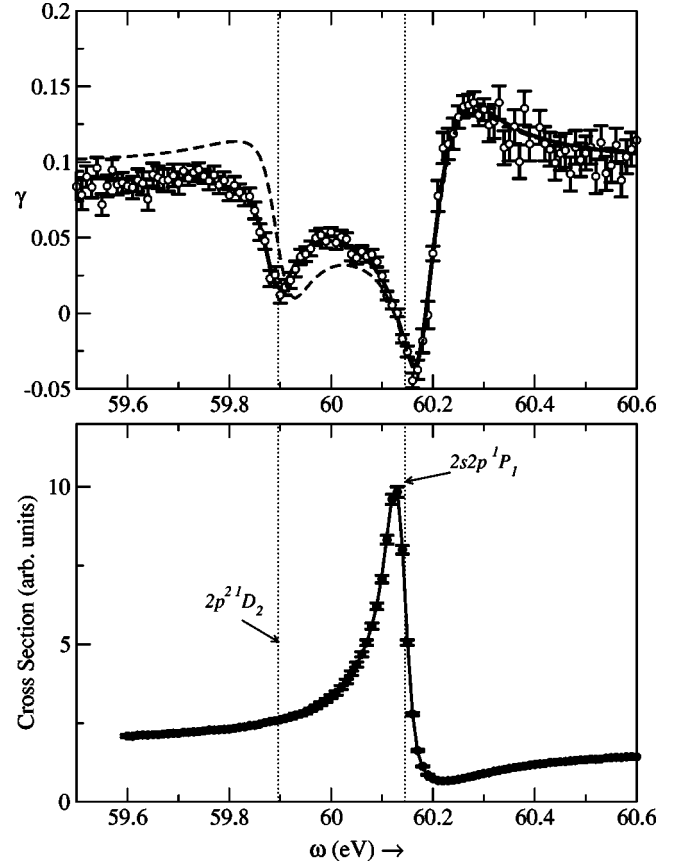


FIG. 3. (Color online) Energy dependence of the total cross section (bottom) and asymmetry parameter γ (top) in the region of the helium $(2s2p)^1P_1$ and $(2p^2)^1D_2$ autoionizing levels. The dashed curve shows the *ab initio* prediction, using Eq. (11) and the theoretical parameters described in the text and convoluted with the experimental resolution. The data and statistical errors are indicated in each figure as discrete points. The fits, described in text, are shown as solid lines.

ment with the best values of those parameters available in the literature (see Table I). The quality of the fit with parameters consistent with previous measurements further confirms our bandpass determination.

As can be seen from Fig. 3, although the influence of the quadrupole resonance is not evident in the total cross section (lower panel), both the dipole and the quadrupole resonances

TABLE I. Helium autoionizing levels and relevant parameters obtained from the literature and present experimental results. The energies (ω_ℓ), widths (Γ_ℓ), and q_ℓ are prior experimental values [21,40]; q_2 [41,42] and the unperturbed continuum phase shifts (δ_ℓ) [43,44] are theoretical values.

	ℓ	ω_ℓ (eV)	Γ_ℓ (meV)	q_ℓ	$\delta_\ell - \delta_1$ (radians)
$2s2p^1P_1$	1	60.150(4)	37.6(2)	-2.73(4)	0
This work			37.9(10)	-2.74(5)	
$2p^2^1D_2$	2	59.91(2)	72(18)	-1.0	-0.3028
This work		59.905(5)	57(3)	-0.25(7)	-0.234(38)

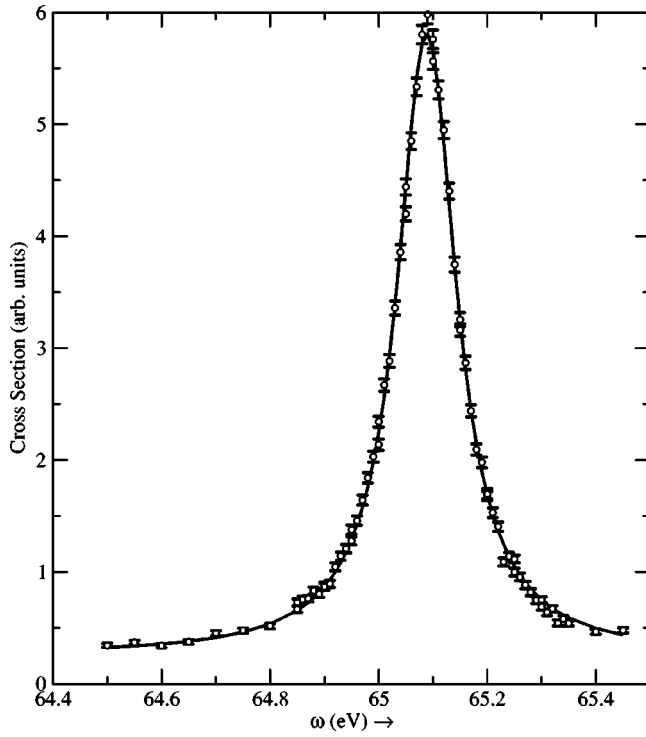


FIG. 4. (Color online) Energy dependence of the measured cross section for the xenon $4d^9 5s^2 5p^6 6p^1 P_1^o$ autoionization resonance. The data are indicated as open circles with statistical errors. The fit, described in text, is shown as a solid line.

produce distinct features in the angular asymmetry parameter γ (upper panel). The variation of the interference term across the 1D_2 resonance is quite large—approximately an order of magnitude larger than that seen in a previous investigation of nondipole asymmetries in autoionization of a quadrupole resonance in Cd [45].

Note that, in this resonance region, γ^R is both positive and negative. Amusia *et al.* [12] note that, for the nonresonant process in He, the photoelectron moves away from the ion in an almost Coulombic potential and γ is therefore always positive; the presence of autoionization modifies the effective potential that the photoelectron sees, and this allows γ^R to be negative. At the energy $\varepsilon_1 = -q_1$ where the amplitude of the dipole resonance passes through zero, it seems that the value of γ^R would be infinite; in actual fact, very close to this energy, expression (4) is modified [as described by Eq. (A2)] becoming instead $\gamma \sim D/Q$ and thus remains finite. Furthermore, in the experiment, the finite energy resolution also leads to a finite measured quantity.

Keeping the dipole resonance parameters fixed at the values determined previously, the data in Fig. 3 were best fitted with γ^R as described in Appendix B to yield the quadrupole resonance parameters shown in Table I. The resulting fit is shown in the upper panel of Fig. 3. In addition, the nonresonant asymmetry γ_0 was also determined from the fit and found to be 0.096(2), in a good agreement with the theoretical prediction of ≈ 0.1 [12] described above. The normalized χ^2 value for this fit was 0.93.

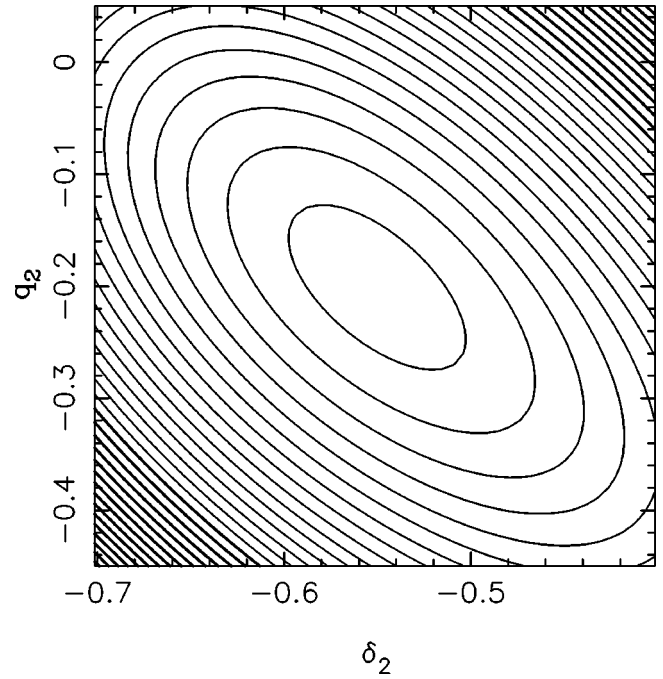


FIG. 5. (Color online) Correlation between q_2 and δ_2 fitting parameters in the χ^2 surface.

Prior to the experiment, the resonant variation of γ was estimated using Eq. (11) and values for the resonance parameters taken from published experimental and theoretical results. This prediction is shown as the dashed curve in Fig. 3, and those resonance parameters are compared with our fitted results in Table I. The previous experimental values of resonance positions, widths, and q_1 are taken from Refs. [21,40]. q_2 is taken from calculated values of the electron scattering quantity $q_2(K)$. In the limit of small momentum transfer K , this is the same as the electric quadrupole value q_2 ; this follows from the fact that the Born radial matrix element in the spherical Bessel function $j_2(Kr) \propto r^2$ as $K \rightarrow 0$ [46]. The Born calculations by Lhagva and Hehmedeh [41] and by Kheifets [42] are in good agreement yielding $q_2 \approx -1$. The Ep, Ed phase shifts have been calculated by Tweed and Langlois [43] and Lhagva [44] for various values of E ; both calculations are in excellent agreement in the energy range of interest. The values given in Table I were obtained by linear interpolation and are essentially constant over the autoionizing resonances. With this procedure, $\delta_1 = -0.3287$.

While the phase shift difference $\delta_2 - \delta_1$ we find only differs from the predicted value by less than 2σ , the shape parameter q_2 is substantially different. As seen in Fig. 5, there is a negative correlation between these two parameters in the fit. As a result, as seen in this figure, further decreasing the phase shift to the theoretical value of $\delta_2 - \delta_1 = -0.3028$ (i.e., $\delta_2 = -0.6315$) would result in an even more positive value of q_2 , a significant departure from theory.

Using the resonance parameters determined in the fits, we have computed the individual bracketed terms in Eq. (11) and show those in Fig. 6(b). Whereas the energy dependence of the total cross section is determined solely by the square of the dipole matrix element [Fig. 6(d)], that of the γ param-

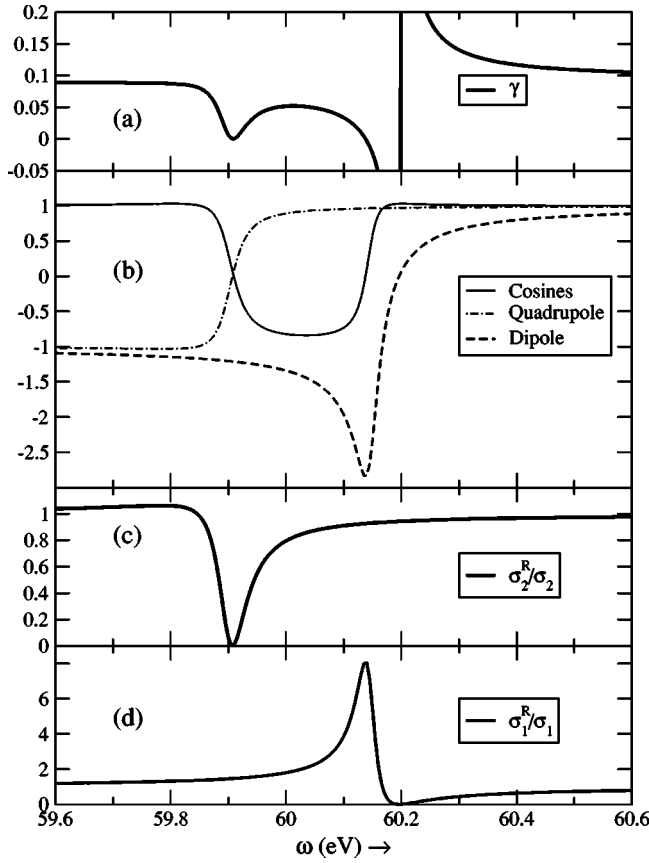


FIG. 6. (Color online) Energy dependence of the various dimensionless terms in Eq. (11) computed using the fitted parameters. Panel (a) shows the value of γ , while (b) shows the three bracketed ($\{\}$) terms in Eq. (11). Panels (c) and (d) show the energy dependence of Eq. (10) for the quadrupole and dipole resonance cross sections, respectively.

eter [Fig. 6(a)] is affected by the interplay among the phase-shift difference and the two matrix elements. These produce a local minimum in γ at the quadrupole resonance position. The γ at the quadrupole resonance shows a minimum of ~ 0 because both the \mathcal{Q} matrix element and the phase shift terms in the numerator of Eq. (11) cross zero and change sign at ω_2 as a consequence of the small magnitude of q_2 , and hence the product is always positive definite. At the energy $\varepsilon_1 = -q_1$ that the amplitude of the dipole resonance passes through zero, the value of γ changes sign as confirmed by this experiment. The energy dependence of the quadrupole cross section [Fig. 6(c)] exhibits the characteristic dip of a window resonance.

A powerful feature of the present experiment lies in the ability to obtain the relative continuum phase shift $\delta_2 - \delta_1$, which is a fitting parameter in Eq. (11). This is possible because of the strong energy dependence of γ^R [Eq. (11)]; away from resonance, the form of γ [Eq. (4)] does not permit the separate determination of both magnitude and phase from experiment. The technique of using the *shape* of an interference feature to obtain phase information has been used previously in an $(e,2e)$ experiment [27,28]. There have also been recent suggestions of techniques to accomplish the same in photoionization [47,48], but to the best of our

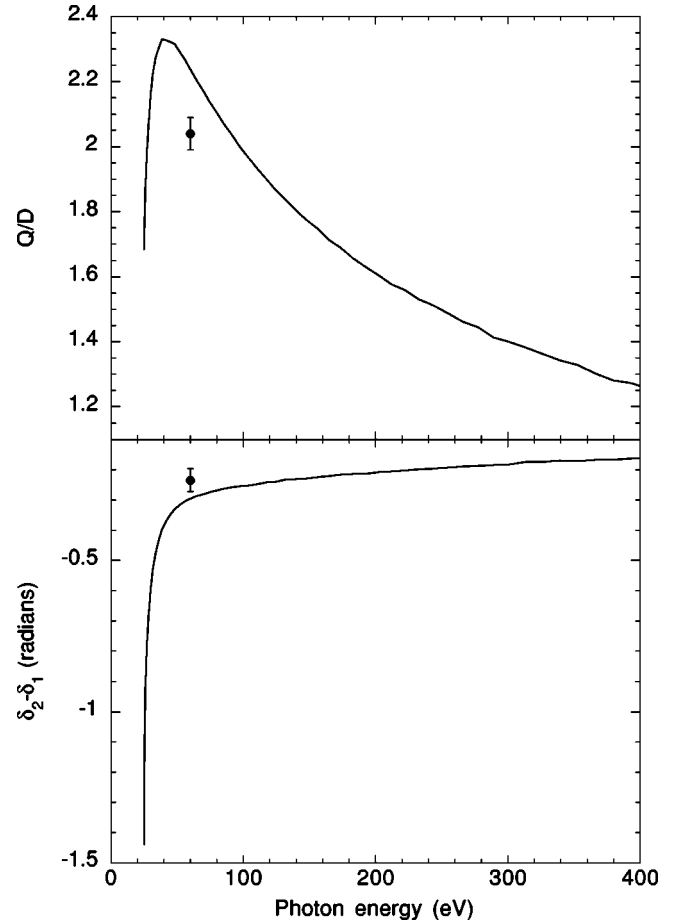


FIG. 7. (Color online) Energy dependence of the difference between quadrupole and dipole phase shifts ($\delta_2 - \delta_1$) in radians (bottom) and the ratio of \mathcal{Q}/D in atomic units (top) predicted by the RPAE calculations. The filled circles show the corresponding quantities extracted from the fits to our data in the resonance region.

knowledge this is the first time this has been realized experimentally. As seen in Table I, we find $\delta_2 - \delta_1$ to be $-0.234(38)$. Combining this value with the experimentally determined value of γ_0 and using Eq. (4), we also determine the radial matrix element ratio to be $\mathcal{Q}/D = 2.04(5)$ at 60 eV photon energy. These experimental results are shown in Fig. 7 along with the predicted energy dependence of the corresponding quantities as given by the RPAE calculations performed here. The product of the factors \mathcal{Q}/D and $\cos(\delta_2 - \delta_1)$ determines γ as shown in Eq. (4) and measurement of these individual quantities can provide a more rigorous test of theory. As seen in Table II, the measured γ_0 is several standard deviations σ below the RPAE prediction. The ratio

TABLE II. Experimental and theoretical (RPAE) values for the principal quantities in Eq. (4) at 60.2 eV photon energy.

	γ_0	\mathcal{Q}/D	$\cos(\delta_2 - \delta_1)$
Expt.	0.096(2)	2.04(5)	0.973(9)
RPAE	0.104	2.24	0.957

Q/D is found to be nearly 4σ below theory, while the cosine factor is roughly 2σ higher than predicted.

C. Comparison with $(e,2e)$ experiments

It is interesting to compare our experiment in the He 1D_2 and 1P_1 resonance region with the equivalent electron scattering experiments. In our photoelectron experiment, the pure dipole-quadrupole interference term may be unambiguously determined from the fore-aft asymmetry in the angular distribution; this is possible because higher-order multipoles are negligible at 60 eV photon energy. This is not true for the $(e,2e)$ experiments. Even at the highest electron impact energy of 400 eV [49], many multipoles are present and fore-aft asymmetry is due to the sum of all the possible odd parity cross terms; it is therefore not possible to isolate the dipole-quadrupole interference contribution. It is also not possible to obtain a meaningful q value for a resonance since the observed asymmetry is due to contributions from *all* multipoles—not just the resonant channel. $(e,2e)$ spectra are therefore analyzed in terms of a generalized triple differential cross section which contains three parameters to describe the collision dynamics [49]. A comparison of theory and experiment is a comparison of calculated and fitted values of these parameters.

The values of q_2 and Γ_2 (Table I) obtained from our photoelectron experiment have implications for both $(e,2e)$ theory and experiment. A calculation of He $(e,2e)$ processes requires two ingredients: He wavefunctions for all the states involved, and a theory of electron impact ionization. Until now a comparison of calculated and experimental parameters is essentially a test of a convolution of scattering theory and wave functions. Our experimental value of q_2 provides an independent test of He wave functions (and correlations) since the electric quadrupole transition operator is known exactly. As can be seen in Table I, the current theoretical values [41,42] of the electric quadrupole q_2 [obtained from $(e,2e)$ calculations in the low momentum transfer limit; see above] substantially differ from the experimental value.

When extracting the dynamic parameters from experimental $(e,2e)$ spectra, it is necessary to know the widths of the resonances. Our more accurate value of $\Gamma_2 = 57(3)$ meV is considerably smaller than the previously used value of $72(18)$ meV (Table I); this result may affect the values of other fitted parameters. The experimental analysis of the $(e,2e)$ data used a cross section formalism that assumed no overlap between the 1D_2 and 1P_1 resonances. While it does not affect photoionization experiments, Lhagva [44] has investigated the consequence of such an overlap in $(e,2e)$ experiments and found it to be important for specific kinematic conditions where the 1P_1 and 1D_2 yields were comparable; the smaller 1D_2 level width that we find clearly affects such calculations.

V. CONCLUSIONS

We have reported our measurements of the forward-backward asymmetry of photoelectron angular distributions produced in the vacuum ultraviolet photoionization of he-

lium. Off resonance, the energy dependence of this asymmetry is generally well represented by the RPAE calculations presented here. In the region of the $2s2p\ ^1P_1$ and $2p^2\ ^1D_2$ autoionizing resonances, these data have allowed us to extract the Fano resonance parameters for the quadrupole resonance. Furthermore, the strong energy dependence of the asymmetry permitted an experimental determination of the matrix element ratio Q/D and the relative continuum phase difference $\delta_2 - \delta_1$. Further measurements of the other He quadrupole autoionization resonances would help to elucidate the comparison to theory. The experimental measurements of these quantities can provide a rigorous test, not previously available, of such calculations.

ACKNOWLEDGMENTS

This work was supported by the Chemical Sciences, Geosciences, and Biosciences Division of the Office of Basic Energy Sciences, Office of Science, U.S. Department of Energy, under Contract No. W-31-109-Eng-38. N.L.S.M. and the UNLV group acknowledge support by the National Science Foundation under Grant Nos. PHY-99-87861 and PHY-01-40375, respectively. We are grateful for the help and hospitality of the staff at the Synchrotron Radiation Center. The University of Wisconsin SRC is supported by National Science Foundation Grant No. DMR-0084402. M.Ya.A. and L.V.C. are grateful to the International Science and Technology Center for support under Project No. 1358.

APPENDIX A: γ FOR VANISHING \mathcal{D}

When the dipole amplitude vanishes at the energy $\varepsilon_1 = -q_1$ in Eq. (10), Eq. (4) is inappropriate since it results from factoring out the dipole cross section. Experimentally, however, the total cross section includes all multipoles. In such circumstances, a better quantity to compare with experiment is the γ , defined by factoring the total cross section in Eq. (3) rather than just the dipole part. In our case, this means including the $O(\alpha^2)$ quadrupole contribution in the total cross section and Eq. (4) then becomes

$$\begin{aligned} \gamma &= 3\alpha\omega \frac{QD}{\mathcal{D}^2 + \frac{1}{4}\alpha^2\omega^2 Q^2} \cos(\delta_2 - \delta_1) \\ &= 3\alpha\omega \frac{Q/D}{1 + \left(\frac{\alpha\omega}{2}\right)^2 \left(\frac{Q}{D}\right)^2} \cos(\delta_2 - \delta_1). \end{aligned} \quad (\text{A1})$$

In the limit $\mathcal{D} \gg \alpha Q$, this reduces to Eq. (4). However, when $\mathcal{D} \ll \alpha Q$, as in the case of the dipole resonance at $\varepsilon_1 = -q_1$, this becomes

$$\gamma = \frac{12}{\alpha\omega} \frac{D}{Q} \cos(\delta_2 - \delta_1). \quad (\text{A2})$$

APPENDIX B: CONVOLUTION

To fit the measured γ values, it is necessary to properly account for the beam line bandpass. To do this, consider the idealized experiment where γ , within a multiplicative constant, is determined by the ratio of cross sections measured with infinite resolution as

$$\gamma = \frac{\sigma_f - \sigma_b}{\sigma_f + \sigma_b} = \frac{\sigma_f - \sigma_b}{\sigma}, \quad (\text{B1})$$

where $\sigma_{f,b}$ are the differential cross sections measured in the forward and backward hemispheres and $\sigma = \sigma_f + \sigma_b$. In contrast to this idealized situation, experimentally we determine γ_{exp} with finite resolution and hence use energy-averaged cross sections:

$$\gamma_{\text{exp}} = \frac{\overline{\sigma_f - \sigma_b}}{\overline{\sigma}}. \quad (\text{B2})$$

Multiplying Eq. (B1) by σ and then energy averaging gives

$$\overline{\gamma\sigma} = \overline{\sigma_f - \sigma_b}. \quad (\text{B3})$$

Finally, dividing by $\overline{\sigma}$ yields

$$\frac{\overline{\gamma\sigma}}{\overline{\sigma}} = \frac{\overline{\sigma_f - \sigma_b}}{\overline{\sigma}}, \quad (\text{B4})$$

which is equivalent to the expression for γ_{exp} in Eq. (B2). Thus, in order to compare computed values of γ to experiment, we energy average our derived γ values by using Eqs. (10) and (11) and forming the convolution integrals

$$\mathfrak{J}_\sigma(\omega) = \int G(\epsilon) \sigma_1^R(\omega + \epsilon) d\epsilon, \quad (\text{B5a})$$

$$\mathfrak{J}_{\gamma\sigma}(\omega) = \int G(\epsilon) \sigma_1^R(\omega + \epsilon) \gamma^R(\omega + \epsilon) d\epsilon, \quad (\text{B5b})$$

where $G(\epsilon)$ is the beam line bandpass function determined previously. The convoluted γ is then given by

$$\overline{\gamma^R} = \frac{\mathfrak{J}_{\gamma\sigma}}{\mathfrak{J}_\sigma}. \quad (\text{B6})$$

-
- [1] J.W. Cooper, in *Photoionization and Other Probes of Many-Electron Interactions*, edited by F. Wuilleumier (Plenum, New York, 1976), p. 31.
- [2] M.O. Krause, *Phys. Rev.* **177**, 151 (1969).
- [3] F. Wuilleumier and M.O. Krause, *Phys. Rev. A* **10**, 242 (1974).
- [4] H.A. Bethe and E.E. Salpeter, *Quantum Mechanics of One and Two-Electron Atoms* (Plenum, New York, 1977).
- [5] P.S. Shaw, U. Arp, and S.H. Southworth, *Phys. Rev. A* **54**, 1463 (1996).
- [6] B. Krässig, M. Jung, D.S. Gemmell, E.P. Kanter, T. LeBrun, S.H. Southworth, and L. Young, *Phys. Rev. Lett.* **75**, 4736 (1995).
- [7] M. Jung, B. Krässig, D.S. Gemmell, E.P. Kanter, T. LeBrun, S.H. Southworth, and L. Young, *Phys. Rev. A* **54**, 2127 (1996).
- [8] P. Auger and F. Perrin, *J. Phys. Radium* **8**, 93 (1927).
- [9] M.Ya. Amusia and N.A. Cherepkov, *Case Stud. At. Phys.* **5**, 47 (1975), and references therein.
- [10] O. Hemmers, M. Blackburn, T. Goddard, P. Glans, H. Wang, S.B. Whitfield, R. Wehlitz, I.A. Sellin, and D.W. Lindle, *J. Electron Spectrosc. Relat. Phenom.* **123**, 257 (2002).
- [11] A. Derevianko, W.R. Johnson, and K.T. Cheng, *At. Data Nucl. Data Tables* **73**, 153 (1999).
- [12] M.Ya. Amusia, A.S. Baltenkov, L.V. Chernysheva, Z. Felfli, and A.Z. Msezane, *Phys. Rev. A* **63**, 052506 (2001).
- [13] J.H. Scofield, *Phys. Rev. A* **40**, 3054 (1989).
- [14] A. Bechler and R.H. Pratt, *Phys. Rev. A* **39**, 1774 (1989).
- [15] A. Bechler and R.H. Pratt, *Phys. Rev. A* **42**, 6400 (1990).
- [16] J.W. Cooper, *Phys. Rev. A* **47**, 1841 (1993).
- [17] W. Heisenberg, *Z. Phys.* **39**, 499 (1926).
- [18] G. Tanner, K. Richter, and J.-M. Rost, *Rev. Mod. Phys.* **72**, 497 (2000).
- [19] R.P. Madden and K. Codling, *Phys. Rev. Lett.* **10**, 516 (1963).
- [20] M. Domke, K. Schulz, G. Remmers, G. Kaindl, and D. Wintgen, *Phys. Rev. A* **53**, 1424 (1996).
- [21] K. Schulz, G. Kaindl, M. Domke, J.D. Bozek, P.A. Heimann, A.S. Schlachter, and J.M. Rost, *Phys. Rev. Lett.* **77**, 3086 (1996).
- [22] M. Domke, C. Xue, A. Puschmann, T. Mandel, E. Hudson, D.A. Shirley, G. Kaindl, C.H. Greene, H.R. Sadeghpour, and H. Petersen, *Phys. Rev. Lett.* **66**, 1306 (1991).
- [23] M. Domke, G. Remmers, and G. Kaindl, *Phys. Rev. Lett.* **69**, 1171 (1992).
- [24] E. Sokell, A.A. Wills, J. Comer, and P. Hammond, *J. Phys. B* **29**, L83 (1996).
- [25] M.K. Odling-Smee, E. Sokell, P. Hammond, and M.A. Macdonald, *Phys. Rev. Lett.* **84**, 2598 (2000).
- [26] B. Krässig, E.P. Kanter, S.H. Southworth, R. Guillemin, O. Hemmers, D.W. Lindle, R. Wehlitz, and N.L.S. Martin, *Phys. Rev. Lett.* **88**, 203002 (2002).
- [27] N.L.S. Martin, D.B. Thompson, R.P. Bauman, and M. Wilson, *Phys. Rev. Lett.* **72**, 2163 (1994).
- [28] N.L.S. Martin, D.B. Thompson, R.P. Bauman, and M. Wilson, *Phys. Rev. A* **50**, 3878 (1994).
- [29] M.Ya. Amusia, A.S. Baltenkov, Z. Felfli, and A.Z. Msezane, *Phys. Rev. A* **59**, R2544 (1999).
- [30] U. Fano, *Phys. Rev.* **124**, 1866 (1961).
- [31] U. Fano and J.W. Cooper, *Phys. Rev.* **137**, A1364 (1965).
- [32] U. Fano and J.W. Cooper, *Rev. Mod. Phys.* **40**, 441 (1968).
- [33] A.F. Starace, *Phys. Rev. A* **16**, 231 (1977).
- [34] N.M. Kabachnik and I.P. Sazhina, *J. Phys. B* **9**, 1681 (1976).
- [35] M.Ya. Amusia, V.K. Ivanov, and V.K. Dolmatov, *Pisma. Zh. Tekh. Fiz.* **6**, 1465 (1980) [*Sov. Tech. Phys. Lett.* **6**, 1465 (1980)].
- [36] B. Krässig, J.-C. Bilheux, R.W. Dunford, D.S. Gemmell, S. Hasegawa, E.P. Kanter, S.H. Southworth, L. Young, L.A. LaJohn, and R.H. Pratt, *Phys. Rev. A* **67**, 022707 (2003).

- [37] D.L. Ederer and M. Manalis, *J. Opt. Soc. Am.* **65**, 634 (1975).
- [38] K. Codling, in *Photoionization and Other Probes of Many-Electron Interactions*, edited by F. Wuilleumier (Plenum, New York, 1976), p. 111.
- [39] M. Jurvansuu, A. Kivimäki, and S. Aksela, *Phys. Rev. A* **64**, 012502 (2001).
- [40] J. van den Brink, G. Nienhuis, J. van Eck, and H. Heideman, *J. Phys. B* **22**, 3501 (1989).
- [41] O. Lhagva and L. Hehmedeh, *J. Phys. B* **27**, 4623 (1994).
- [42] A.S. Kheifets, *J. Phys. B* **26**, 2053 (1993).
- [43] R.J. Tweed and J. Langlois, *J. Phys. B* **20**, 5213 (1987).
- [44] O. Lhagva, *Z. Phys. D: At., Mol. Clusters* **23**, 321 (1992).
- [45] N.L.S. Martin, D.B. Thompson, R.P. Bauman, C.D. Caldwell, M.O. Krause, S.P. Frigo, and M. Wilson, *Phys. Rev. Lett.* **81**, 1199 (1998).
- [46] R.D. Cowan, *The Theory of Atomic Structure and Spectra* (University of California Press, Berkeley, 1981).
- [47] I.A. Vartanyants and J. Zegenhagen, *Solid State Commun.* **113**, 299 (1999).
- [48] J.M. Feagin, *Phys. Rev. Lett.* **88**, 043001 (2002).
- [49] A. Crowe, D.G. McDonald, S.E. Martin, and V.V. Balashov, *Can. J. Phys.* **74**, 736 (1996).